

Kerr and free-carrier ultrafast all-optical switching of GaAs/AlAs nanostructures near the three-photon edge of GaAs

Alex Hartsuiker* and Philip Harding

*Center for Nanophotonics, FOM Institute for Atomic and Molecular Physics (AMOLF),
Kruislaan 407, 1098 SJ Amsterdam, The Netherlands*

Yoanna-Reine Nowicki-Bringuier and Jean-Michel Gérard
*CEA/INAC/SP2M, Nanophysics and Semiconductor Laboratory,
17 rue des Martyrs, 38054 Grenoble Cedex, France*

Willem L. Vos

*Center for Nanophotonics, FOM Institute for Atomic and Molecular Physics (AMOLF),
Kruislaan 407, 1098 SJ Amsterdam, The Netherlands and*

*Complex Photonic Systems (COPS), MESA+ Institute for Nanotechnology,
University of Twente, The Netherlands*

(Dated: May 31, 2018, version 5)

Abstract

We performed non-degenerate pump-probe experiments on a GaAs/AlAs photonic structure. We switched the photonic properties using the optical Kerr effect and free carriers excited by three photon absorption. From these measurements we extracted the non-degenerate Kerr coefficients over a broad wavelength range and we extracted the three photon absorption coefficient for GaAs at three wavelengths in the near infrared. We show that the optical Kerr effect is large enough to switch a cavity resonance with a high Q ($Q > 1000$) photonic cavity.

*Electronic address: hartsuiker@amolf.nl

I. INTRODUCTION

Exciting prospects arise when photonic structures are switched on ultrafast timescales. For example, switching would allow the capture or release of photons from photonic band gap cavities [1], which is relevant to solid-state slow-light schemes [2]. Switching the directional properties of photonic crystals also leads to fast changes in the reflectivity, where interesting changes have been reported for Bragg stacks [3, 4], 2D photonic crystals [5, 6, 7], and first-order stop bands of 3D opaline crystals [8, 9]. Ultrafast control of the propagation of light is essential to applications in active photonic integrated circuits [10].

Different mechanisms are possible for switching photonic structures. The switching of photonic structures with free carriers [5, 6, 11, 12] and a phase transition of VO_2 [13] have been reported recently. The disadvantage of a phase transition is that the material changes from a transparent material to a metal, which absorbs light. On the other hand free carrier excitation is ultrafast, but the recombination of the carriers is limited to a picosecond time scale.

With instantaneous switching it would be possible to ultimately control the on- and off-time of the switching event. This is possible with the optical Kerr effect, where the on- and off-time are determined by the pulse duration. This extreme of fast switching can be used for capturing and releasing photons on demand for example in a vertical-cavity surface emitting laser [14].

In order to release photons from cavity, the refractive index change induced with the optical Kerr effect should be large enough. To shift the cavity resonance by one linewidth the refractive index change should be equal to $\frac{\Delta n'}{n'} = \frac{1}{Q}$ [15]. Thus for an experiment with a cavity having a quality factor Q of 1000, this means a refractive index change of 0.1%. It is well known (see [1]) that the magnitude of the refractive index change by the Kerr effect is much smaller than the change due to a free carrier switch.

A problem which occurs at coincidence of pump and probe pulse is non-degenerate two-photon absorption [11]. Here, a probe photon is absorbed together with a pump photon when the summed energy of the pump and probe exceed the bandgap energy. The change in imaginary part of the refractive index can be large compared to the change in the real part, giving rise to absorptive changes in the optical properties.

In this work we propose a method to decrease non-degenerate two photon absorption at pump and probe coincidence. Because of this, we are able to show that the optical Kerr effect is large enough to switch a cavity resonance with a moderate Q of 1000 or higher. We derive the Kerr

coefficient and the three photon absorption coefficient over a broad wavelength range.

II. EXPERIMENTAL

A. Sample

Our structure consists of a GaAs λ thick layer (277 nm thick) sandwiched between two Bragg stacks consisting of 12 and 16 pairs of $\lambda/4$ thick layers of nominally pure GaAs or AlAs. The sample is grown with molecular beam epitaxy at 550°C to optimize the optical quality [16]. For experiments outside the present scope the sample was doped with 10^{10}cm^{-2} InGaAs/GaAs quantum dots, which hardly influence our experiment [17].

B. Optical measurements

Our setup consists of two independently tunable optical parametric amplifiers (OPA, Topas), that are the sources of the pump and probe beams. The setup has been described in [18] therefore we present only a brief outline here. The OPAs have pulse durations $\tau_p = 140 \pm 10$ fs. The pump beam has a much larger Gaussian focus of 113 μm full width at half maximum than the probe beam (28 μm), ensuring that only the central flat part of the pump focus is probed. A versatile measurement scheme was developed to subtract the pump background from the probe signal, and to compensate for possible pulse-to-pulse variations in the output of our laser [18]. Separately, continuous-wave (cw) reflectivity was measured with a broad band white light setup with a resolution of ~ 0.2 nm [19].

In this work we varied the pump wavelength from 2000 nm to 2400 nm in steps of 200 nm. The probe wavelength was varied independently of the pump wavelength between 1150 nm and 1650 nm, with steps of 5 nm. Measured data was corrected for dispersion in the system.

III. RESULTS

A. Linear reflectivity

Figure 1C shows the measured linear reflectivity spectrum of our sample and a transfer matrix (TM) calculation [20]. The transfer matrix calculation including the dispersion of GaAs [21] and

AlAs [22] reproduces the experimental resonance, stopband, and Fabry- Pérot fringes. The only free parameters in the model were the thicknesses of the GaAs ($d_{\text{GaAs}} = 69.2 \text{ nm}$) and AlAs ($d_{\text{AlAs}} = 81.0 \text{ nm}$), which agree to the measured values. The reflectivity spectrum shows the stopband with cavity resonance and Fabry-Pérot fringes. The spectrum can be divided into two spectral regions, namely 'Absorptive' (right, densely hatched) and 'Dispersive' (left, hatched), referring to the expected behavior if pump and probe coincide.

The origin of the absorption is explained in figure 1A and 1B, which show schematic energy diagrams at coincidence of pump and probe. The regions are separated at a wavelength which corresponds to the bandgap at a pump wavelength of 2400 nm. In the densely hatched spectral region, the pump and probe photon will be absorbed since the sum of the photon energies is higher than the bandgap of GaAs. In the sparsely hatched (dispersive) spectral region however, the sum of pump and probe photon energies is not larger than the bandgap of GaAs. Therefore absorption is low in this region and behavior at coincidence is therefore mainly dispersive. Only the real part of the refractive index n' changes.

The origin of the dispersion is the optical Kerr effect. There will be a change in the real part of the refractive index (n'), due to the pump field. The edge of the hatched regions in figure 1C will shift to the red at a pump wavelength of 2000 nm, indicating that we expect absorption in a large part of the spectrum. The behavior at coincidence is therefore mainly absorptive, meaning a change in the imaginary part of the refractive index, (n'').

We focus in this work on the spectral region indicated by the black rectangle. In this region we expect to observe effects of the optical Kerr effect but only little absorption at 2400 nm pump wavelength, while we expect mainly absorption at 2000 nm pump wavelength.

B. Ultrafast switched reflectivity

The two plots in figure 2 show the differential reflectivity measured at 2000 nm, $I_{\text{pump}} = 90 \text{ GW/cm}^2$ (A) and 2400 nm, $I_{\text{pump}} = 95 \text{ GW/cm}^2$ (C) pump wavelength as a function of probe wavelength and delay. Cross sections of figure 2A and C are given in figure 2B and D respectively.

A fringe pattern is visible in figure 2A and C for coincidence of pump and probe and for positive delay. Figure 2B and D show cross sections of 2A and C. The sign difference of differential reflectivity between pump and probe overlap and positive delay is apparent and is a result from the

fringe patterns at coincidence and positive delay, which are spectrally shifted with respect to each other. This indicates that the switch mechanism at coincidence is different from the free-carrier mechanism at positive delay.

At a pump wavelength of 2000 nm we expect a change in n'' , since we are in the absorptive regime. At 2400 nm pump wavelength we expect a change in n' and a negligible change in n'' , since we are in the dispersive region (see figure 1).

The differential reflectivity at positive delay is caused by excited free carriers. Figure 3 shows the power dependence of differential reflectivity ($\Delta R/R$) at positive delay. There is a linear relation between the differential reflectivity and the power cubed, as shown in figure 3. We therefore conclude that the differential reflectivity is caused by free carriers generated by a three photon absorption process.

C. Interpretation of time-resolved reflectivity

The fringe pattern in figure 2A and 2C results from Fabry-Pérot interferences within the stack forming the optical microcavity. A change in n' modifies the optical thickness of the GaAs layers; it induces a spectral shift of the Fabry-Pérot fringes, which results in a periodic differential reflectivity. A change in n'' decreases the modulation depth of the Fabry-Pérot fringes.

The differential reflectivity due to a change in the real part of the refractive index depends on measured intensities as follows:

$$\frac{\Delta R}{R}(\tau, \omega_{pr}, \omega_{pu}) = \frac{I_{pu}(\tau, \omega_{pr}, \omega_{pu}) - I_{unpu}(\omega_{pr})}{I_{unpu}(\omega_{pr})} \quad (1)$$

Where $\frac{\Delta R}{R}$ is the differential reflectivity, τ is the delay between pump and probe, ω_{pr} is the probe frequency, ω_{pu} is the pump frequency, I_{unpu} is the reflectance measured if the structure is unpumped and I_{pu} is the reflectance measured if the structure is pumped.

In case of a change in the real part of the refractive index, the fringe pattern shifts spectrally $\Delta\omega_{pr} = \alpha n'$, with α a proportionality constant that depends on the exact structure of the fringe pattern. I_{pu} is then given by:

$$I_{pu}(\tau, \omega_{pr}, \omega_{pu}) = I_{unpu}(\omega_{pr} + \Delta\omega_{pr}(\tau, \omega_{pu})) \quad (2)$$

Which can be written as

$$I_{pu}(\tau, \omega_{pr}, \omega_{pu}) = I_{unpu}(\omega_{pr}) + \frac{\partial I_{unpu}(\omega_{pr})}{\partial \omega_{pr}} \Delta\omega_{pr}(\tau, \omega_{pu}), \quad (3)$$

which yields a differential reflectivity:

$$\frac{\Delta R}{R}(\tau, \omega_{pr}, \omega_{pu}) = \frac{1}{I_{unpu}(\omega_{pr})} \frac{\partial I_{unpu}(\omega_{pr})}{\partial \omega_{pr}} \Delta \omega_{pr}(\tau, \omega_{pu}) \quad (4)$$

Equation 4 shows that in the case of a change in the real part of the refractive index a large differential reflectivity will be measured where the unpumped reflectivity has a large derivative, which is spectrally between successive maxima and minima of the Fabry-Pérot fringes. This is illustrated in figure 4. In the case of a change in n'' the modulation depth of the fringe pattern is affected, while in the case of a change in n' the position of the fringe pattern is shifted. For this reason the differential reflectivity has maxima at different positions making it possible to distinguish between a purely dispersive and a purely absorptive regime.

Figure 5 shows a TM calculation of the differential reflectivity spectrum of the planar microcavity. The intensity profile in the structure is homogeneous, leading to a homogeneous refractive index change. The intensity profile is homogenous since we pump at a long wavelength in the three photon absorption regime. The homogeneity length ([23]) is longer than our sample. Figure 5 shows a comparison between the measured and calculated differential reflectivity pattern. Comparing the measured and calculated patterns shows that the positions of the peaks and troughs in the differential reflectivity pattern near zero delay, are caused by a change in the imaginary part of the refractive index (n'') in the case of 2000 nm pump and a change in the real part of the refractive index (n') in the case of 2400 nm pump. We conclude that in the case of 2400 nm pump wavelength the fringe pattern near zero delay in the differential reflectivity originates from a Kerr switch, since the process is ultrafast, instantaneous with the laser pulse and is dispersive. In case of 2000 nm pump wavelength the fringe pattern originates from non-degenerate two photon absorption. Furthermore we see a slight deviation of our model near the blue side of the spectrum, indicating some dispersion in the nonlinear effect. We further conclude from figure 5 that absorption can be neglected at 2400 nm pump wavelength, while dispersion can be neglected at 2000 nm pump wavelength.

By varying the size of the change in n' we extracted the change in refractive index at each wavelength. The results are plotted together with dispersion curves in figure 6. Figure 6 shows no change in refractive index for a negative delay (A), a positive change for zero delay (B) and a negative change for positive delay (C). Furthermore there is a good agreement between the data and the dispersion of the optical Kerr effect [24] and the dispersion of the free carrier excitation [18].

The scattered symbols deviating strongly from the theoretical model can be attributed to small differences in shape of the measured and calculated reflectivity spectrum. A slight deviation is amplified by the fitting procedure since we extract the refractive index change by fitting the differential reflectivity at one wavelength position.

Figure 6B shows that the change in refractive index induced by the optical Kerr effect is in the order of 0.1%. This is large enough to switch a cavity with a moderate Q of 1000.

D. Non linear coefficients GaAs

1. Kerr coefficient n_2 for GaAs

The non-degenerate Kerr coefficient n_2 can directly be extracted from the data $\Delta n'$ in figure 6 using the relation [24, 25],

$$n_2 = \frac{\Delta n'}{2I_0} \quad (5)$$

where I_0 is the pump intensity. Since n_2 scales with E_{gap}^{-4} [24], the contribution of AlAs is only 20% of the total n_2 . For simplicity we therefore assume that mainly the GaAs is switched.

The resulting Kerr coefficients are plotted in figure 7. Figure 7 shows the raw data extracted from figure 6 (open circles) and the data averaged over the width of a fringe (solid squares). The order of magnitude of n_2 is $10^{-4} GW cm^{-2}$. The non-degenerate Kerr coefficient decreases with increasing wavelength. This dispersive behavior was already observed in figure 5.

The values of n_2 measured in our non-degenerate pump-probe experiment are similar to the ones reported in the literature for degenerate pump-probe experiments [26, 27, 29]. We find this surprising since we pump at a wavelength twice as long as in the degenerate case. This result enables us to modify efficiently the refractive index with a far detuned pump wavelength.

2. Three photon absorption coefficient γ for GaAs

Figure 6 shows that we are able to derive a carrier density from the measured change in refractive index with the use of the Drude model. We will discuss in this section the three photon absorption coefficient γ .

Figure 8 shows the three photon absorption coefficient γ as a function of pump wavelength. The order of magnitude of γ is $10^{-3} cm^3 GW^{-2}$. Our data are two orders of magnitude smaller

than the values reported in the literature [29], measured with the z-scan method. We attribute this difference to the fact that our data have been obtained on an epitaxially-grown GaAs/AlAs heterostructure, instead of a GaAs wafer obtained with a different technique.

The three photon absorption coefficient decreases as a function of wavelength since the summed energy of a pump and probe photon, and therefore the probability of generating an electron hole pair, decreases with increasing wavelength. The three photon absorption edge is 2580 nm.

IV. CONCLUSION

We showed switching of the fringes of a GaAs/AlAs planar optical microcavity using the optical Kerr effect and three photon absorption.

From the switching measurements we extracted the non-degenerate Kerr coefficients over a broad wavelength range. Furthermore we extracted the three photon absorption coefficients for three different wavelengths in the near infrared.

We conclude from our results that it is possible to switch a cavity with a Q higher than 1000, using the optical Kerr effect. The refractive index change is in the order of the required 0.1%.

Acknowledgments

We want to thank Allard Mosk and Patrick Johnson for stimulating discussion. This research was supported by NanoNed, a nanotechnology programme of the Dutch Ministry of Economic Affairs, and by a VICI fellowship from the "Nederlandse Organisatie voor Wetenschappelijk Onderzoek" (NWO) to WLW. This work is also part of the research programme of the "Stichting voor Fundamenteel Onderzoek der Materie" (FOM), which is financially supported by the NWO.

-
- [1] P. M. Johnson, A. F. Koenderink, W. L. Vos, *Phys. Rev. B* **66**, 081102(R) (2002)
 - [2] M. F. Yanik, S. Fan, *Phys. Rev. Lett.* **92**, 083901 (2004)
 - [3] A. Haché, M. Bourgeois, *Appl. Phys. Lett.* **77**, 4089 (2000)
 - [4] S. R. Hastings, M. J. A. de Dood, H. Kim, W. Marshall, H. S. Eisenberg, D. Bouwmeester, *Appl. Phys. Lett.* **86**, 031109 (2005)
 - [5] S. W. Leonard, H. M. van Driel, J. Schilling, R. B. Wehrspohn, *Phys. Rev. B* **66**, 161102(R) (2002)

- [6] H. W. Tan, H. M. van Driel, S. L. Schweizer, R. B. Wehrspohn, U. Gösele, *Phys. Rev. B.* **70**, 205110 (2004)
- [7] A. D. Bristow, J.-P. R. Wells, W. H. Fan, A. M. Fox, M. S. Skolnick, D. M. Whittaker, A. Tahraoui, T. F. Krauss, J. S. Roberts, , *Appl. Phys. Lett.* **83**, 851 (2003)
- [8] D. A. Mazurenko, R. Kerst, J. I. Dijkhuis, A. V. Akimov, V. G. Golubev, D. A. Kurdyukov, A. B. Pevtsov, A. V. Sel'kin, *Phys. Rev. Lett.* **91**, 213903 (2003)
- [9] C. Becker, S. Linden, G. von Freymann, M. Wegener, N. Tétreault, E. Vekris, V. Kitaev, G. A. Ozin, *Appl. Phys. Lett.* **87**, 091111 (2005)
- [10] H. Nakamura, Y. Sugimoto, K. Kanamoto, N. Ikeda, Y. Tanaka, Y. Nakamura, S. Ohkouchi, Y. Watanabe, K. Inoue, H. Ishikawa, K. Asakawa, *Opt. Express* **12**, 6606 (2004)
- [11] P. J. Harding, T. G. Euser, Y.-R. Nowicki-Bringuier, J.-M. Gérard, W. L. Vos *Appl. Phys. Lett.* **91**, 111103 (2007)
- [12] X. Hu, P. Jiang, C. Ding, H. Yang, Q. Gong, *Nat. Phot.* **2**, 185 (2008)
- [13] D. A. Mazurenko, R. Kerst, J. I. Dijkhuis, A. V. Akimov, V. G. Golubev, A. A. Kaplyanskii, D. A. Kurdyukov, A. B. Pevtsov, *Appl. Phys. Lett.* **86**, 041114 (2005)
- [14] S. G. Hense, M. Wegener, *Phys. Rev. B* **55**, 9255 (1997)
- [15] T. G. Euser, A. J. Molenaar, J. G. Fleming, B. Gralak, A. Polman, W. L. Vos, *Phys. Rev. B* **77**, 115214 (2008)
- [16] J.-M. Gérard, D. Barrier, J. Y. Marzin, R. Kuszelewicz, L. Manin, V. Costard, V. Thierry-Mieg, T. Rivera, *Appl. Phys. Lett.* **69**, 449 (1996)
- [17] The maximum unbroadened refractive index change of the dots amounts to only 10^{-8} , while the absorption at resonance is less than 0.02 cm^{-1} .
- [18] T. G. Euser, Ph.D. thesis, University of Twente ISBN 978-90-365-2471-1 (2007)
- [19] M. S. Thijssen, R. Sprik, J. E. G. J. Wijnhoven, M. Megens, T. Narayanan, L. Lagendijk, W. L. Vos, *Phys.Rev.Lett.* **83**, 2730 (1999)
- [20] M. Born, E. Wolf, *Principles of Optics: Electromagnetic Theory of Propagation, Interference and Diffraction of Light.* (Cambridge University Press 1999)
- [21] J. S. Blakemore, *J. Appl. Phys.* **53**, R123 (1982)
- [22] R. E. Fern, A. Onton, *J. Appl. Phys.* **42**, 3499 (1971)
- [23] T. G. Euser, W. L. Vos, *J. Appl. Phys* **97**, 043102 (2005)
- [24] M. Sheik-Bahae, J. Wang, E. W. van Stryland, *IEEE J. of Quantum Electron.* **30**, 249 (1994)

- [25] R. W. Boyd, *Nonlinear Optics*, Academic Press ISBN 0-12-121680-2, pp 162 (1992)
- [26] M. Dinu, F. Quochi, H. Garcia, *Appl. Phys. Lett.* **82**, 2954 (2003)
- [27] T. G. Ulmer, R. K. Tan, Z. Zhou, S. E. Ralph, R. P. Kenan, C. M. Verber, *Opt. lett.* **24**, 756 (1999)
- [28] A. A. Said, M. Sheik-Bahae, D. J. Hagan, T. H. Wei, J. Wang, J. Young, E. W. Van Stryland, *J. Opt. Soc. Am. B* **9**, 405 (1992)
- [29] W. C. Hurlbut, Y.-S. Lee, K. L. Vodopyanov, P. S. Kuo, M. M. Fejer, *Opt. Lett.* **32**, 668 (2007)

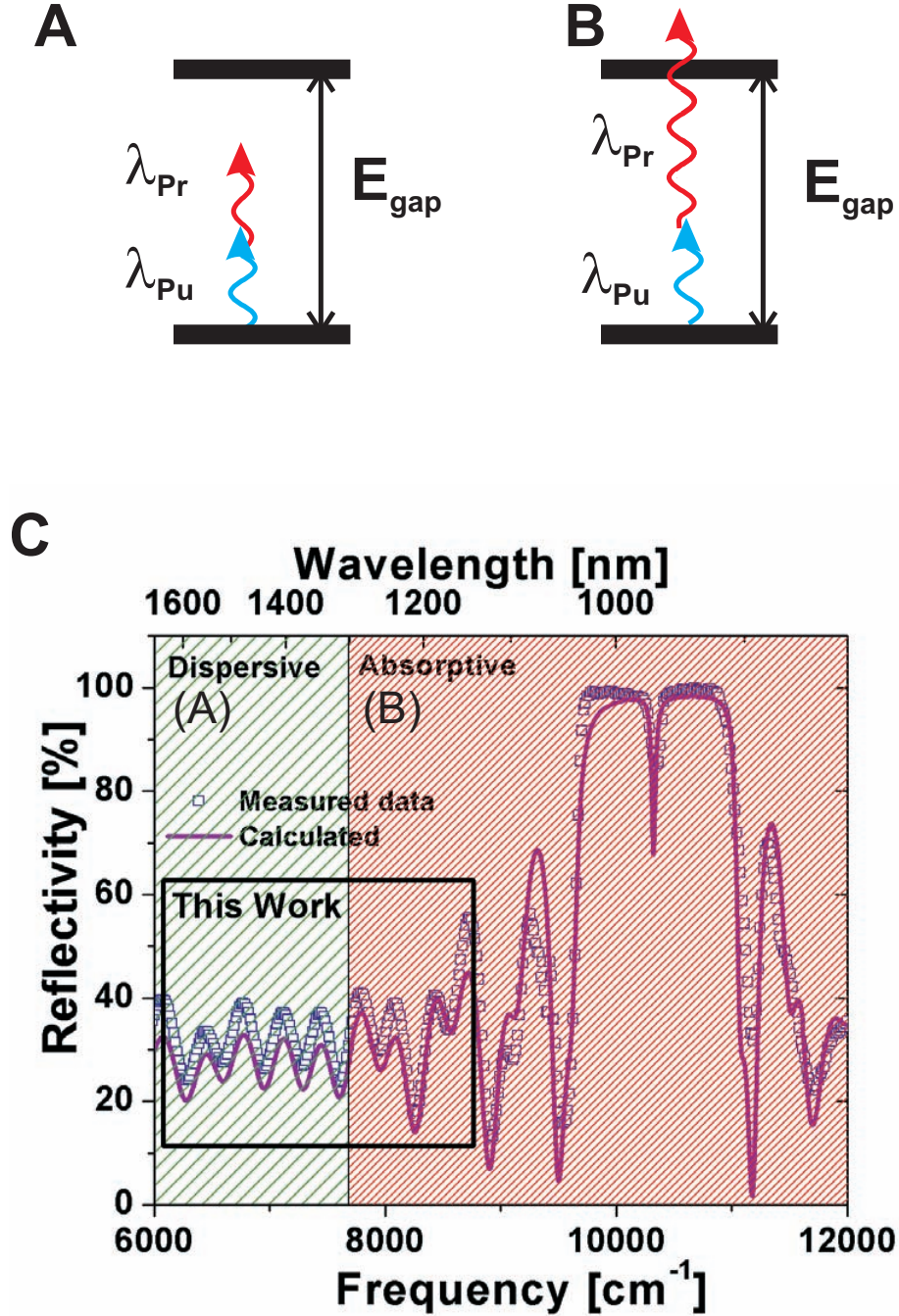


FIG. 1: (A,B) Schematic energy diagrams of GaAs. E_{gap} is the electronic bandgap of GaAs, λ_{Pr} is the probe wavelength and λ_{Pu} is the pump wavelength. The edge between diagram A and B is at a probe wavelength of 1510 nm and 1340 nm at pump wavelengths of 2000nm and 2400nm respectively. In the dispersive spectral region the summed energy of a pump and a probe photon is smaller than the bandgap, while the summed energy is larger in the absorptive spectral region. We present measurements in the spectral region indicated with a square, to obtain a change in the real part of the refractive index. (C) Linear reflectivity spectrum and transfer matrix calculation of the GaAs/AlAs structure. The trough at 980 nm is due to the cavity resonance of the lambda thick GaAs layer. The hatched regions are based on a pump wavelength of 2400nm. The slight difference in amplitude of the measured and calculated reflectivity on the red side of the stopband is

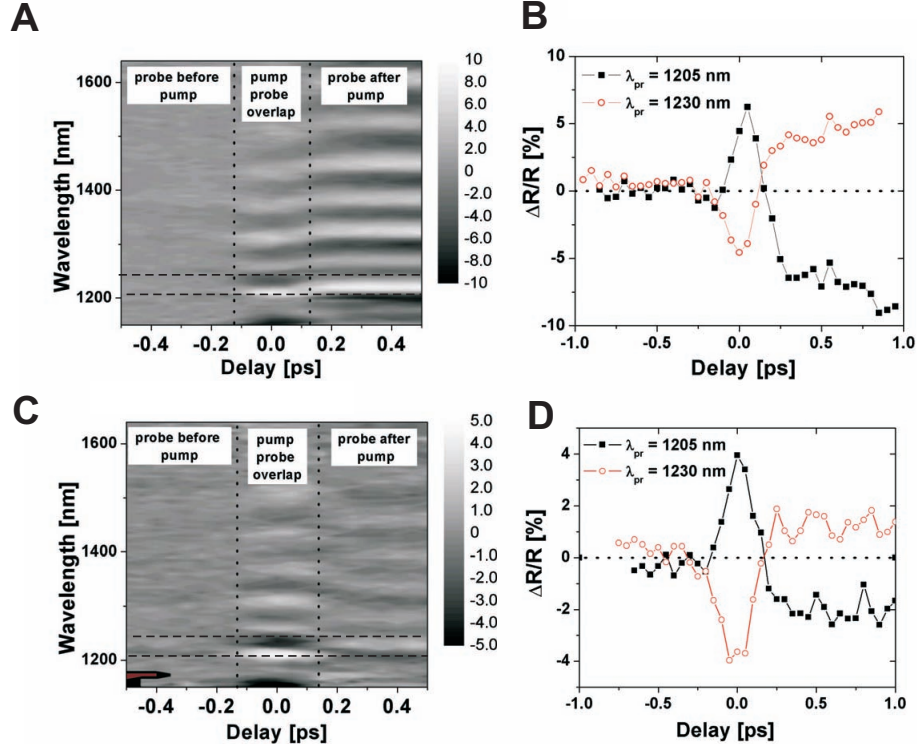


FIG. 2: Differential reflectivity per wavelength as a function of delay between pump and probe pulse. At negative delays the pump hits the sample before the probe. The scans were measured at different pump wavelengths. (A) $\lambda_{pump} = 2000$ nm, $I_{pump} = 90$ GW/cm², (C) $\lambda_{pump} = 2400$ nm, $I_{pump} = 95$ GW/cm². Cross cuts indicated by dashed lines in A and C are shown in figure B and D respectively. Figure A and C show a fringe pattern indicating a shift of the Fabry-Pérot fringes. The cross sections B and D show that the sign of the differential reflectivity at coincidence is different from the sign at positive delay.

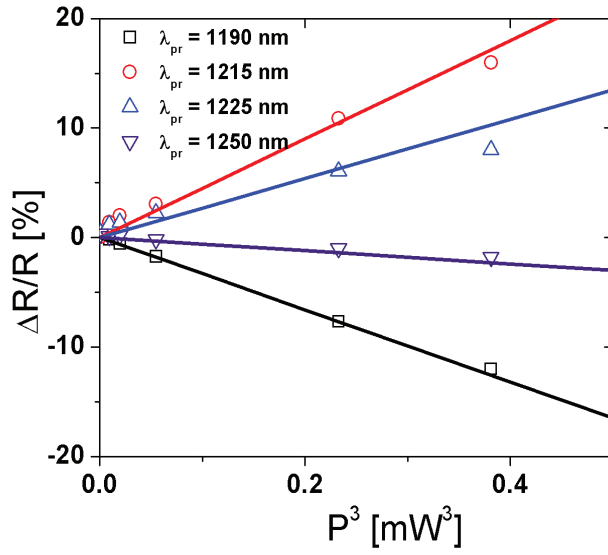


FIG. 3: *Differential reflectivity at positive delay measured at different probe wavelengths at a pump wavelength of 2000 nm. The differential reflectivity is plotted as a function of pump power cubed. The relation between the differential reflectivity at positive delay and the power cubed is linear. We conclude that the carriers are solely generated through a three photon process.*

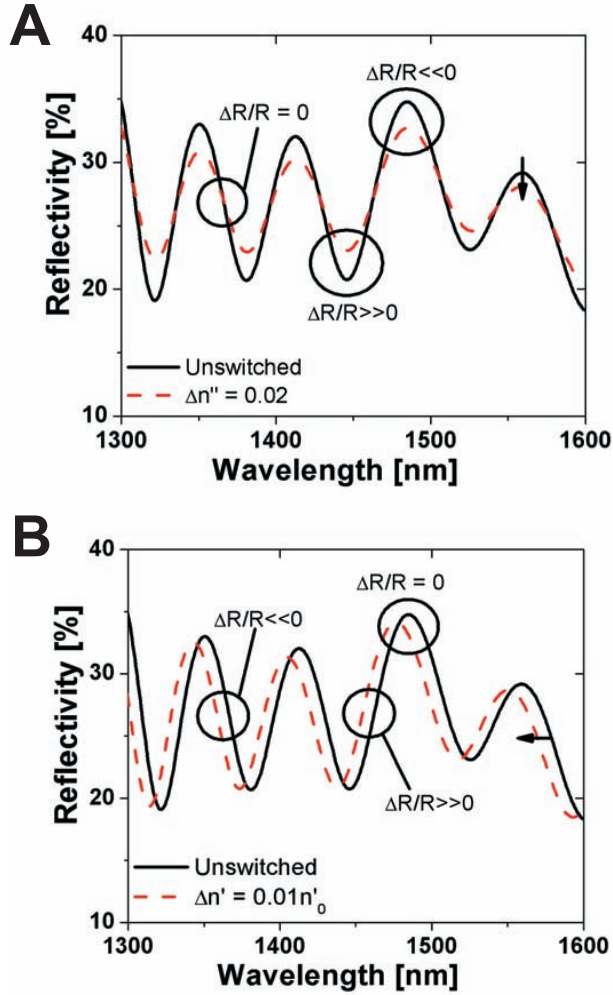


FIG. 4: Switched and unswitched reflectivity for a change in the n'' (A) and a change in n' (B). Figure A shows that the introduction of absorption mainly affects the modulation depth of the fringes. A change in n' causes a shift of the fringe pattern (B). The differential reflectivity has maxima at different spectral positions, which makes it possible to distinguish between a purely dispersive and a purely absorptive regime.

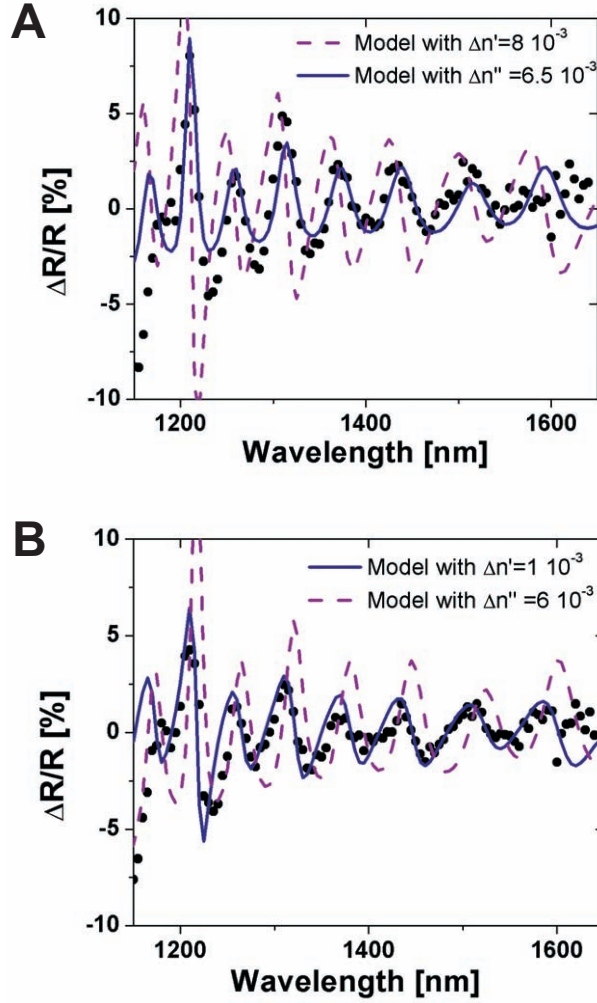


FIG. 5: Cross section of figure 2 (black solid circles) showing the differential reflectivity $\Delta R/R$ as a function of probe wavelength at pump-probe coincidence ($\Delta t = 0$ ps). The structure was pumped at 2000 nm (A) and 2400 nm (B). The solid and dashed lines are results from transfer matrix calculations. In (A) the dashed line represents a change in the real part of the refractive index while the solid line represents a change in the imaginary part of the refractive index. This is the other way around in (B): dashed represents a change in imaginary part, while solid represents a change in the real part of refractive index. As expected we see mainly a change in the imaginary part of the refractive index at 2000 nm pump and a change in n' at 2400 nm. Furthermore our model slightly deviates near the blue side of the spectrum.

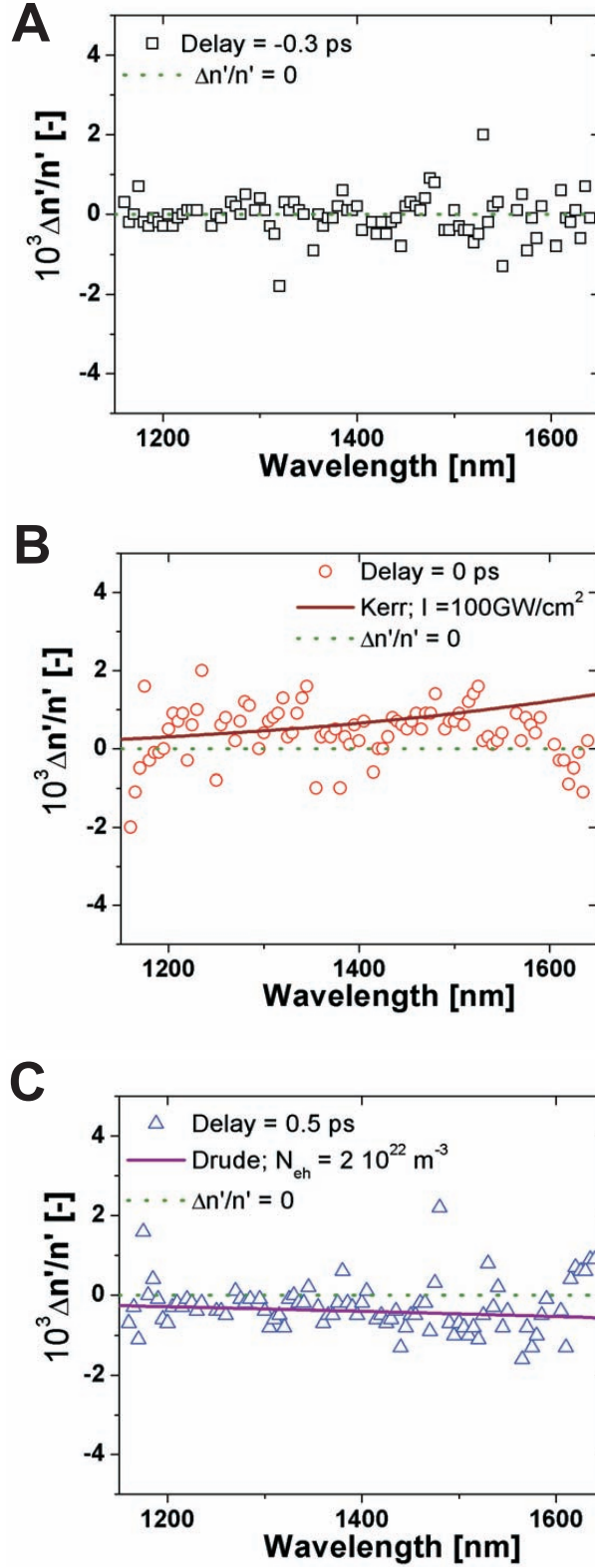


FIG. 6: Relative change of refractive index due to a 2400 nm pump as a function of probe wavelength at a delay of -0.3 ps (A), 0 ps (B) and 0.5 ps (C). The dashed line in all three cases represent no change in refractive index. The solid line in (B) represents the dispersion of the change in refractive index from [24]. The solid line in (C) is calculated with the Drude model for free carriers [18]. Points obtained from spectral regions close to extrema of the fringes were removed, because of their poor precision.

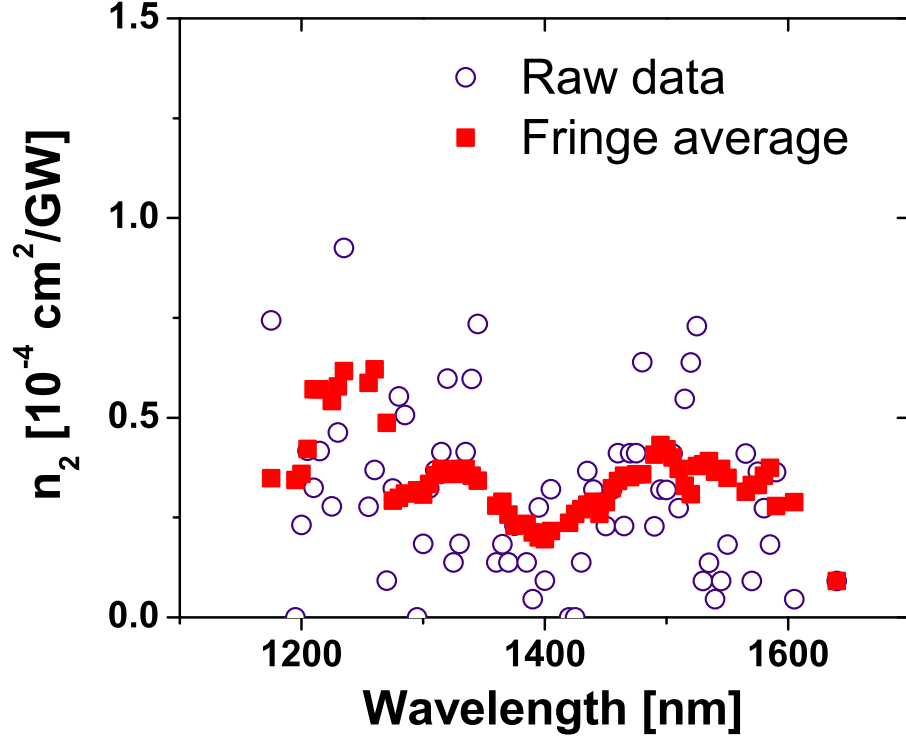


FIG. 7: Measured non-degenerate Kerr coefficient n_2 as a function of probe wavelength (open circles). We averaged the data over the period of one fringe, since the coefficients are correlated within this fringe period (solid squares). We observe dispersion in n_2 towards the blue side of the spectrum as expected from figure 5.

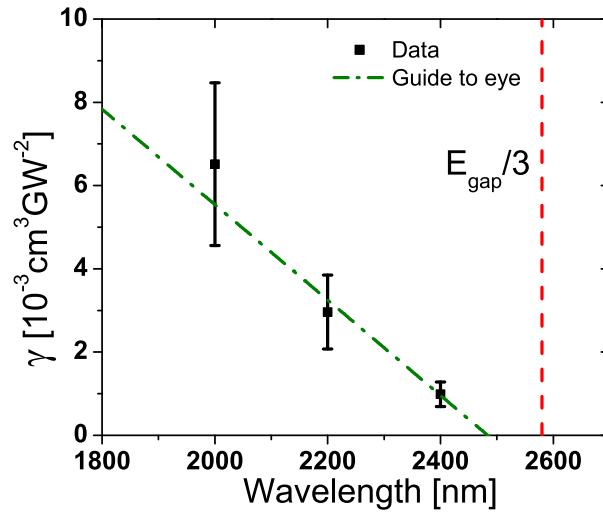


FIG. 8: Three photon absorption coefficient as a function of wavelength extracted from the differential reflectivity data. The relative error of 30 % is indicated.